Effects of Metallic Nanoalloys on Dye Fluorescence

Cassandre Jenny Dorcéna

Thesis submitted to the faculty of the Virginia Polytechnic Institute and State University
in partial fulfillment of the requirements for the degree of

Master of Science
in
Electrical Engineering

Dr. Kathleen Meehan, Chair
Dr. Sanjay Raman, Member
Dr. Yong Xu, Member
Dr. Brian J. Love, Member

September 5, 2007
Blacksburg, VA

Keywords: metallic nanoparticles, surface plasmon resonance,
surface enhanced fluorescence, fluorescence quenching

Effects of Metallic Nanoalloys on Dye Fluorescence

Cassandre Jenny Dorcéna

ABSTRACT

Metallic nanoparticles (NPs) are exploited for their ability to interact with organic compounds and to increase significantly the fluorescence intensity and the photostability of many fluorescent dye molecules. Metal enhanced fluorescence (MEF) is therefore widely investigated for biosensing applications. When used in immunoassays, silver island films (SIFs) could augment the fluorescence intensity of fluorescein by a factor of seventeen; SIFs were also able to double or triple the emission intensity of cyanine dyes which are commonly used in (deoxyribonucleic acid) DNA microarrays. The emission intensity of indocyanine green – widely used as a contrast agent in medical imaging – was about twenty times higher in the proximity of SIFs.

This enhancement phenomenon - due to the surface plasmon polaritons associated with the metallic NPs – can be explained by energy transfer from the metal NPs to the fluorescent dye molecules or by a modified local electromagnetic field experienced by the fluorophores in the vicinity of metal surfaces.

Our research focused on the optical characterization of colloidal gold-silver alloy NPs containing different ratios of gold and silver ($Au_{1.00}$-$Ag_{0.00}$, $Au_{0.75}$-$Ag_{0.25}$, $Au_{0.50}$-$Ag_{0.50}$, and $Au_{0.25}$-$Ag_{0.75}$), as well as their interaction with three fluorophores: rose bengal, rhodamine B, and fluorescein sodium. Depending upon the dye quantum yield and its concentration in solution, enhancement or quenching of fluorescence was obtained. Thus, a three to five times increase in fluorescence intensity was observed in a 2.0 mM solution of rose bengal with all nanoalloys, a slight enhancement of fluorescence (1.2 – 1.6 times) was noticed in a 0.13 mM solution of rhodamine B with all four types of NPs, and fluorescence quenching occurred in all the fluorescein-NP solutions regardless of the dye concentration.

DEDICATION

This thesis is dedicated to my best friend and beloved fiancé, Eric Masson, for his tender love and invaluable support. You have initiated me into the uncertain and exciting world of research; you have shared my joys and my deceptions; you have been my strength during this journey at Virginia Tech. I will forever be grateful!

I also dedicate this work to my dear parents, Nicole and Dominique Dorcéna, without whom I could have never reached this point in my life. Thank you for your love, support, and sacrifices!

How to forget my wonderful sisters Béatrice and Carine who have never ceased to encourage me through their numerous telephone conversations? Thank you so much for your moral support!

ACKNOWLEDGEMENTS

I would like to thank my thesis advisor, Dr. Kathleen Meehan, for her advice, guidance, and her willingness to meet with me whenever I needed help.

I would also like to thank Dr. Sanjay Raman, Dr. Yong Xu, and Dr. Brian J. Love for accepting to serve on my committee and for their helpful suggestions during the writing of my thesis.

Finally, I would like to thank Mr. William C. Miles and Dr. Stephen McCartney for their assistance with dynamic light scattering measurements and transmission electron micrographs.

Financial assistance for this project has been provided by a grant from Luna Innovations, Inc., entitled “Enhancement of Fluorescence in Protease Assays for Biowarfare Toxins”.

TABLE OF CONTENTS

TABLE OF FIGURES

1 Introduction

Metal colloids have fascinated people for centuries. Indeed, they have been used to make some colored glasses [1]. Colloidal gold was at the origin of the color admired in medieval cathedral windows and, until the eighteenth century, was believed to rejuvenate and prolong life [2]. The origin of the color of the colloids was first recognized by Faraday in 1857 [3]. Localized surface plasmons (LSPs) – charge density oscillations across metallic nanoparticles (NPs) and metallic nanostructures [4] – are excited by an incident light impinging on the metal surface at a particular wavelength where resonance occurs. This phenomenon causes strong light scattering and surface plasmon absorption bands, as well as an enhancement of the local electromagnetic field. The wavelength and intensity of the surface plasmon peaks depend on the type of the material, its size and size distribution, and the shape of the nanostructures, as well as the medium in which they are embedded [5,6]. These various properties of metallic NPs and nanostructures have allowed their use as molecular recognition elements, components in nanoscale optical devices, and in sensors and biosensors [7]. This chapter emphasizes the biosensing applications resulting from the interactions between metal NPs and nanostructures with fluorophores. It, thus, shows our motivations for the experiments that will be described and discussed in subsequent chapters.

1.1 Theoretical Overview

Before discussing biosensing applications, we shall briefly review the theory describing the interaction of light with fluorescent dyes and metallic nanoparticles. This theory can be divided into two parts: the effect of the incident light on the metallic NPs and the interaction of the NPs with fluorescent dye molecules [8].

Let us assume a metallic NP, which is composed of a fixed positively charged core and negatively charged free electrons on its surface. By direct illumination of the metallic

NP, a rapid oscillation of the electrons across the NP arises because of the intensity and sinusoidal nature of the electric field. This causes the formation of a dipole (see Figure 1.1). Surface plasmon resonance (SPR) occurs when the oscillator is in resonance with the incident electromagnetic waves [8].

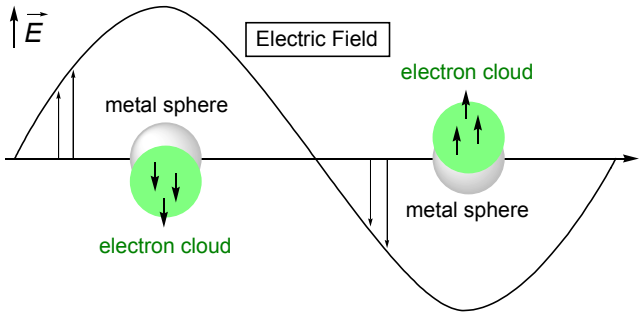

Figure 1.1. Schematic of plasmon oscillation for a sphere, showing the displacement of the conduction electron charge cloud relative to the nuclei. Adapted from [9].

An enhancement of the fluorescence of a dye molecule can occur when the dye is in the vicinity of a metal NP. The increase of the electric field in the proximity of the NP plays a very important role in this phenomenon [8]. The electric field increase, which depends on the shape of the NP, is about two orders of magnitude higher at the surface of the NP relative to the magnitude of the electric field of the photons that illuminated the NP, but the amplitude of the electric field decays as the distance from the NP increases. Let us consider two point charges of opposite signs, +q and –q, located at the positions (d/2, -d/2) on the z axis of a coordinate system as shown below:

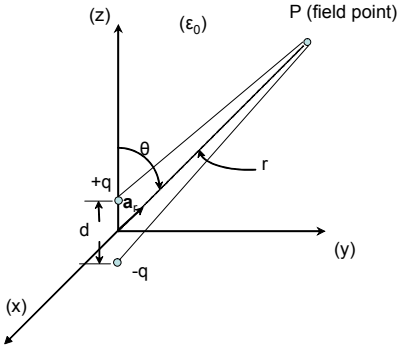

Figure 1.2. Geometry of a static charge dipole. Adapted from [10].

When r >> d, the electric field in spherical coordinates of the fixed dipole charges is given by:

$$\mathbf{E} \cong \frac{qd}{4\pi\varepsilon_0 r^3}\left[\mathbf{a}_r 2\cos\theta + \mathbf{a}_\theta \sin\theta\right] \quad (1.1)$$

where r and θ are spherical coordinate variables, $\mathbf{a}_r$ is a unit vector directed from the point (0,0,0) to the field point P, $\mathbf{a}_\theta$ is a unit vector with respect to θ, and ε_0 is the permittivity of free space. Within few diameters of the NP, the influence of the electric field resulting from the NP's oscillating electrons on fluorescence enhancement decreases significantly.

The accurate interaction of electromagnetic waves and spherical NPs is explained by Mie's theory [11]. As we will see in Chapter Two, the wavelength at which SPR occurs depends on the chemical nature of the NP, its shape, and the environment that surrounds it [8].

A fluorescent dye located in close proximity of the metal NP senses the altered electric field and experiences an enhancement in its fluorescence intensity. This enhancement has two effects: an increase of the molecular population in the excited state and an increase in the quantum efficiency of the fluorophore. Concerning the first effect, the excitation of the fluorescent dye is directly proportional to the square of the intensity of the electric field enhancement [8]. The maximum fluorescence enhancement is obtained when the wavelength at which SPR occurs equals the fluorescent dye absorption wavelength [8]. Concerning the second effect, the quantum yield of the fluorescent dye without other quenching interactions is given by:

$$Q_0 = \frac{\Gamma}{\Gamma + k_{\mathrm{nr}}} \quad (1.2)$$

where Γ is the radiative decay rate and k_{nr} is the nonradiative decay rate [8, 12]. The radiative decay rate is determined by the extinction coefficient of the fluorophore, which is slightly dependent on the medium. Therefore, the radiative decay rate is essentially constant for any given fluorescent dye. In general, the only way to alter the quantum yield of a fluorophore is by changing the nonradiative decay rate k_{nr} [12]. However, the

presence of a nearby metal NP increases the radiative rate by addition of a new radiative channel Γ_m [8, 12]. The quantum efficiency thus becomes [12]:

$$Q_m = \frac{\Gamma + \Gamma_m}{\Gamma + \Gamma_m + k_{nr}} \quad (1.3)$$

In this case, maximum enhancement is achieved when the wavelength at which SPR occurs is equal to the emission wavelength of the fluorescent dye. The fluorescence enhancement is very effective if the dye molecule has a low intrinsic quantum yield Q_0; however, it is not significant for a fluorescent dye with a high intrinsic quantum yield [8]. Other enhancement effects include a decrease of the fluorescence lifetime and an increase in photostability [12]. It is interesting to note that, for metal-dye distances within 5 nm, a quenching effect (a *non*-surface plasmon resonance effect) occurs, which also influences the fluorescence of the dye [8].

1.2 Applications of Metal Enhanced Fluorescence to Biosensing

1.2.1 *MEF in ultra Bright Labeled Proteins: New Class of Probes for Immunoassays and Immunostaining*

Fluorophores have been used as probes in order to determine the amount of antibody present in a sample or the amount of protein bound by an antibody. Therefore, covalently labeled proteins with dye molecules have been extensively used as reactants in immunoassays [13]. Fluorescein is a commonly used fluorophore for this kind of application. However, this dye is often subjected to self-quenching of its fluorescence. This is due to Förster resonance energy transfer between neighboring fluorescein molecules [14]. Consequently, the intensity of the labeled protein decreases with increasing labeling density [15]. It has been reported that most of the self-quenching can be eliminated by placing the labeled protein in the proximity of silver island films (SIFs) [15,16]. It has been speculated that the reduction in self-quenching resulted from an increase in the radiative decay rate [15]. For example, the fluorescence intensity of fluoroescein-5-isocyanate-labeled human serum albumin (FITC-HSA) was examined

when FITC-HSA was bound to glass (quartz) and to SIFs. With a 7:1 labeling ratio (molecules of fluorophores per protein molecule), the emission intensity was about 17 times higher in the presence of SIFs than on glass alone [15] (see Figure 1.3).

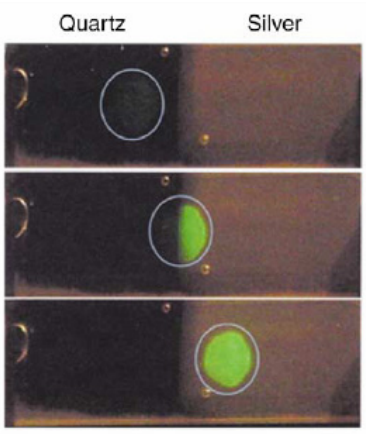

Figure 1.3. Photograph of fluorescein-labeled human serum albumin on quartz and on SIFs as observed with 430 nm excitation and a 480 nm long-pass filter. The excitation was progressively moved from the quartz side to the silver side. Reproduced with permission from [15].

This decrease in self-quenching resulted from an increase in radiative decay rate (see equation 1.3) [13]. It has been concluded that SIFs and most probably colloidal silver could be utilized to obtain ultra bright reagents for use in immunoassays [15].

1.2.2 *MEF in Deoxyribonucleic Acid (DNA) Hybridization for Biotechnological and Diagnostic Applications*

The detection of DNA hybridization [17] is at the core of various biotechnological and diagnostic applications such as gene chips [18], polymerase chain reactions (PCR) [19,20], and fluorescence *in situ* hybridization [21]. It is therefore desirable to use a general approach to detect changes in fluorescence intensity upon hybridization. Silver NPs were used to achieve this goal and to increase the sensitivity of DNA detection [22]. In this method, thiolated oligonucleotide single-stranded DNA was bound to silver particles on a glass substrate. A complementary fluorescein-labeled oligonucleotide (F1-DNA) was added to the sample containing the silver-bound DNA. The proximity of F1-

DNA to silver particles during hybridization with the capture DNA resulted in a decreased fluorescence lifetime and a 12-fold increase in fluorescence intensity [22].

1.2.3 *Metal-Enhanced Fluorescent Probes in DNA Microarrays*

With a few exceptions, every cell of the body has its full set of chromosomes and identical genes. However, only a subset of these genes are turned on or "expressed", giving unique properties to each cell type [23]. Analysis of gene expression is crucial in many areas of biological research since variations in the physiology of an organism or a cell imply variations in the pattern of gene expression [24]. DNA microarray technology is a technique that is widely used in studies of gene expression [25-27]. A DNA microarray (also called gene or genome chip, DNA chip, or gene array) is a collection of microscopic DNA spots onto which DNA single strands containing sequences from thousands of different genes are immobilized [23, 28]. The supports are generally glass microscope slides, silicon chips or nylon membranes. In a DNA microarray, single strands of DNA are fixed to the support in an organized way so that the location of each spot indicates a particular gene sequence [23]. DNA microarrays have the benefit that large sets of gene expression can be found in parallel. This technology exploits the ability of a given mRNA (messenger ribonucleic acid) or single-strand DNA to hybridize to these immobilized gene sequences [24]. Practically, mRNA is purified from a biological sample; the corresponding complimentary DNA (cDNA) is obtained by reverse transcription and linked to a fluorescent dye. Most commonly used fluorophores are cyanine dyes Cy3 and Cy5. After labeling of cDNA, hybridization to the microarray takes place [24]. Computational methods are used to accurately measure the amount of cDNA bound to a specific gene on the microarray. This helps to create a profile of gene expression in the cell [23] (see Figure 1.4).

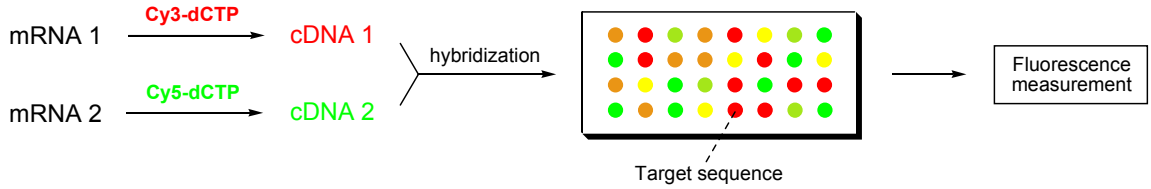

Figure 1.4. Gene expression analysis by DNA microarray technology. mRNA samples are reverse transcribed to cDNA while fluorescently labeled nucleotides are incorporated. The usage of multiple dyes allows the comparison of multiple RNA samples on one single array.

It is desirable to improve the detection of hybridized DNA by using methods that would increase the total emission per labeled DNA and therefore provide better sensitivity [29]. A recent report investigated the effects of SIFs on the emission properties of fluorophore-labeled DNA. The emission intensity of Cy3-DNA and Cy5-DNA doubled and tripled, respectively, on SIFs as compared to quartz slides [29]. An increase in intensity and a decrease in lifetime are consequences of an increase of the radiative decay rate in the proximity of the SIFs [29].

We have seen that fluorescence is a very important technique for DNA sequencing, and genomics. Nevertheless, it is necessary to do further investigations in order to maximize fluorescence in fluorescence-based biochips platforms [8]. Therefore, a recent publication focused on a method based on MEF in order to optimize fluorescence enhancement in sensor detection systems. The fluorescent dye Cy5 commonly utilized in optical immunoassays and whose quantum efficiency is about 0.3, was used in this study [8].

Cy5 has absorption and emission wavelengths in the red region of the electromagnetic spectrum, which is removed from the region of intrinsic fluorescence coming from most biological tissues [8]. Several methods – such as electron beam lithography [30], atom-light interaction lithography [31], electrodeposition of metal NPs [32], and electrochemical template synthesis of metallic NPs [33] – have been used for the synthesis of metal NPs on a support. However, these methods exhibited disadvantages, namely high production cost, significant polydispersity of the NPs, and deficient control of their optical properties in the red region [8]. These handicaps could be overcome by using nanosphere lithography (NSL) for the synthesis of mono-dispersed

metallic NPs whose surface plasmon properties are in the visible and infrared spectrum and whose size can be designed to suit the dye spectral properties [8].

Rectangular glass slides were coated with polystyrene beads (PBs) whose size varied (200 to 500 nm) according to the samples. Then, a silver layer with graduated thickness was deposited and the PBs were removed after sonication of the sample. For the design of enhancement chips, silica was deposited over the substrate containing the NPs. The NPs obtained were triangular in shape, which corresponds to the triangular shape of spaces in the PB mask (see Figure 1.5). Finally, Cy5-labeled DNA dots were printed in the array [8]. The wavelength at which SPR occurred (λ_{res}) was found to depend on the diameter of the PBs. With 500 nm PBs and variable metal thickness, λ_{res} was in the region of absorption and emission of the Cy5 dye (red region) [8]. The maximum enhancement (about 8) occurred when λ_{res} fell between 645 and 695 nm. In this case, the surface plasmon absorption peak corresponded to the absorption and emission wavelength of the Cy5 dye [8].

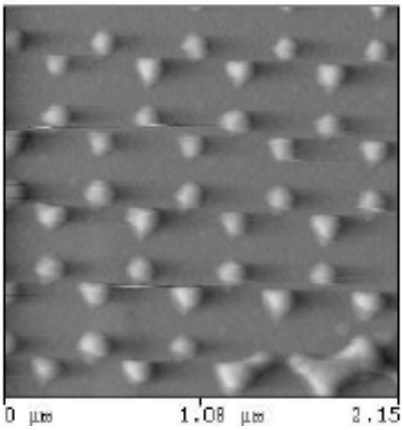

Figure 1.5. Atomic Force Microscope image of triangular shape NPs. Reproduced with permission from [8].

1.2.4 *MEF for Medical Imaging*

Indocyanine green (ICG) is a non-toxic dye [34] that absorbs and emits light in the near infrared spectrum, allowing good light penetration in the biological tissue [35]. This fluorophore (approved by the Food and Drug Administration) has a wide variety of

medical imaging applications such as retinal angiography [35]; assessment of burn depth [36] and exercise physiology [37]; optical detection of tumors [38] and optical tomography [39].

Effects of unsilvered and silvered surfaces on ICG bound to human serum albumin were reported [34]. The silvered surfaces were silver island films deposited on a glass substrate by chemical reduction of silver nitrate with D-glucose under controlled conditions [34]. The diameter of the silver islands ranged from 100 to 500 nm across and about 60 nm high, with some aggregates. It was noticed that the emission intensity of ICG was about 20 times higher in the proximity of SIFs than with the bare quartz surface [34]. This fluorescence enhancement was due to a higher quantum yield and/or rate of excitation of the dye molecule near the silver particles. Moreover, the proximity of ICG to SIFs did not increase the rate of photobleaching [34]. Due to their ability to improve fluorescent dye emission, metal colloids could be used for purposes of injection [13]. In addition to their ability to enhance fluorescence, metallic colloids have good scattering properties [40,41]. Therefore, combining strong scattering with fluorescence enhancement could dramatically improve detection in tissues [34].

1.3 Conclusions and scope of the project

It was shown that metallic NPs possess the ability to enhance the emission intensity of many fluorescent dye molecules. In particular, SIFs located in the proximity of fluorophores such as fluorescein, Cy3, Cy5, and indocyanine green, significantly increased the fluorescence intensity of these organic molecules. Therefore, MEF could be used as a powerful tool in many biosensing applications such as immunoassays, genomics, and medical imaging.

Our work was motivated by the numerous benefits of placing NPs in the vicinity of fluorescent dye molecules. Yet, it did not make use of SIFs but rather of colloidal gold-silver alloy NPs in order to simplify the synthesis of these NPs by eliminating the substrate. Moreover, biological molecules are in general in an aqueous medium. Thus, it is very important to have colloidal systems whose phase is homogeneous with that of the

target molecules. Surface enhanced fluorescence obtained by directly mixing colloidal nanoparticles with the biological molecules can be used to lower the detection limit of target analytes and/or to reduce the number of amplification cycles in polymerase chain reaction (PCR) systems with in situ optical monitoring. The use of metallic colloids to enhance fluorescence of dye molecules is also of importance in high throughput fluorescence-based detection systems where loss of the SIFs from the substrate may occur over time whereas the concentration of colloidal nanoparticles in solution can be easily replenished.

There is a need to understand the optimal conditions for surface enhanced fluorescence of a dye in solution with colloidal nanoparticles. Hence, our research investigated the impact of gold-silver nanoalloys on three particular fluorophores: rose bengal, rhodamine B, and fluorescein sodium where we evaluated the dye-nanoparticle interactions as a function of dye and nanoparticle concentration and as a function of the wavelength of the SPR.

2 Theoretical Background

This chapter describes the theory upon which our research was based. It points out the interaction of light with metallic NPs and the effect of metal NPs on fluorescent dye molecules placed in their vicinity.

2.1 Surface Plasmons or Surface Plasmon Polaritons

The term "surface plasmon" is often used in metal thin films in order to describe the electromagnetic waves that propagate along the interface between a metal film and a dielectric material such as organic films [42a]. The light absorption by metallic thin films results in a coherent motion of electrons at their surface, causing a wave. Therefore, this wave is called a surface plasmon wave.

Three conditions are necessary for the existence of a surface plasmon:

a) the materials meeting at the interface must be of different dielectric constants, ε_d and ε_m, where ε_d is the dielectric constant of the environment, and ε_m, the metal dielectric constant, is equal to the sum of its real and imaginary components $(\varepsilon_m = \varepsilon_1 + i\varepsilon_2)$;

b) $\varepsilon_1 < 0$; and

c) $\varepsilon_1 = -2\,\varepsilon_d$

These conditions can be satisfied simply by putting a metallic film in contact with vacuum, air, or glass. Once these conditions are met, surface plasmons can be appropriately excited.

The excitation of a surface plasmon requires a match between the wave vector of the incident light in the direction of surface plasmon propagation and the wave vector of the surface plasmon expected to be produced, according to the relation:

$$\vec{k}_{light} = \vec{k}_{sp} \quad (2.1)$$

or

$$k_{sp} = k_0 \sqrt{\frac{\varepsilon_m \varepsilon_d}{\varepsilon_m + \varepsilon_d}} \quad (2.2)$$

where k_{sp} is the momentum of the surface plasmon, k_0 is the momentum of light in vacuum, ε_m is the complex dielectric constant of the metal, and ε_d is the complex dielectric constant of the environment in contact with the metal layer.

Electromagnetic waves propagate in a metal film in the frequency and wavelength for which light propagation is forbidden in either of the two media. In other words, light cannot couple directly as a surface plasmon at a flat metal surface. This is because the wavevector $\vec{k}_{sp}$ of the surface plasmon wave is much larger than that of light propagating in air or vacuum [42b]. Hence, no direct excitation of the surface plasmon is possible, and special geometries are required in order to generate a surface plasmon. The Kretschmann configuration of attenuated total reflection (ATR) is widely used for that purpose (see Figure 2.1) [42a]. A microscopic glass slide coated with a metallic thin film (usually a 40-to-50-nm thick gold or silver film) is coupled to a prism through an index matching fluid or a polymer layer. Then a beam of light, whose reflection is controlled, is impinged on the prism. At a particular angle, θ_{sp} the electromagnetic wave couples to the metal-glass interface as a surface plasmon, resulting in a drop in the intensity of the reflected light (the ATR signal). The angle is given by the relation:

$$k_{sp} = k_0 n_p \sin\theta_{sp} \quad (2.3)$$

where k_{sp} is the momentum of the surface plasmon, k_0 is the momentum of light in vacuum, n_p is the refractive index of the prism, and θ_{sp} is the angle of incidence of light needed to generate a surface plasmon.

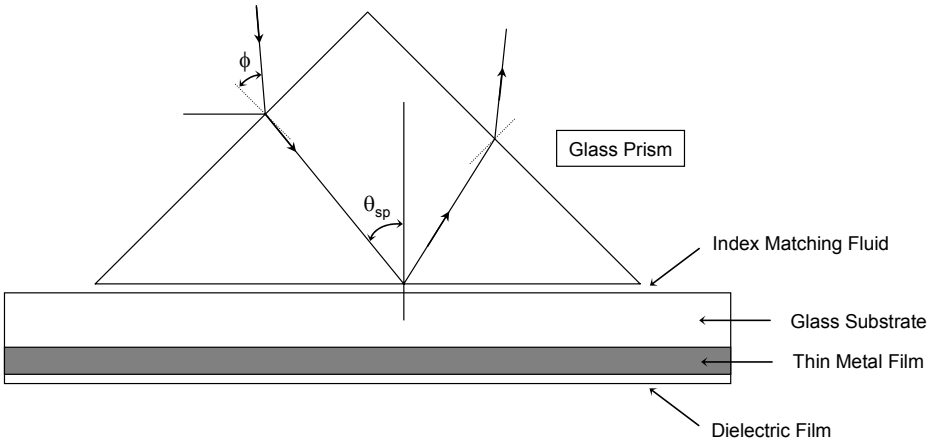

Figure 2.1. Kretschmann configuration used to excite surface plasmons; Φ is the angle of incidence of light at the prism-air interface. Adapted from [42a].

The concept of surface plasmon can also be applied to metallic nanostructures or nanoparticles (NPs), in which case it is often called "localized surface plasmon" since the wave vector of the surface plasmon cannot characterize the movement of the electrons. Optical excitation in NPs produces a collective oscillation of electrons across the NPs, creating a dipole. To excite these localized surface plasmons, no special geometry (such as the Kretschmann configuration) is needed. The specific wavelengths of light absorption necessary to produce plasmon oscillations are called surface plasmon bands or plasmon bands [42c].

A dipole approximation is often used to describe the optical properties of small metallic particles (for which the radius is much smaller than the wavelength of light). This approximation gives rise to an extinction coefficient k_{ex} (measure of both absorption and scattering strengths) of the metal NP by the following relation (adapted from ref. [42g]):

$$k_{ex} = \frac{24\pi^2 r^3 \varepsilon_d^{\frac{3}{2}}}{\lambda} \frac{\varepsilon_2}{\left(\varepsilon_1 + 2\varepsilon_d\right)^2 + \varepsilon_2^2} \quad (2.4)$$

where λ is the wavelength of light, ε_d is the dielectric constant of the surrounding medium, ε_1 and ε_2 represent the real and imaginary parts of the dielectric constant ε_m of the metal ($\varepsilon_m = \varepsilon_1 + i\varepsilon_2$), and r is the radius of the NP. The highest transfer of energy from a photon to the metal NP, causing the oscillation of the electrons, occurs for the

resonance condition: $2\varepsilon_d = -\varepsilon_1$. Surface plasmon resonance (SPR) is then achieved, implying maximum absorption of light. From equation 2.4, we notice that a change in the dielectric constant around the NPs causes a variation in the amplitude and the wavelength of the SPR peak. We also observe that the size of the NPs has a direct impact on the amplitude and the wavelength of the localized surface plasmon peak as both the real and imaginary components of ε_m are a function of the radius of the nanoparticle.

The shape of metal NPs has also an effect on their resonance properties. When particles (like nanorods or ellipsoidal NPs) are nonsymmetrical in shape, they display a SPR peak for each of their dimensions. This is the result of different orientations and magnitudes of the dipoles inside these nonsymmetrical particles. For instance, for a nanorod-shaped metallic NP, the plasmon band shifts into two bands corresponding to the oscillation of free electrons in the longitudinal and transverse directions with respect to the long axis of the nanorod [43]. A spherical NP may have a single plasmon band associated with its singular dimension, *i.e.* its radius.

It is informative to consider that, in a nanoscale material, scattering processes can be observed since light can be scattered outside the NP (in which the number of atoms is very limited compared to a bulk material). This leads us to talk about Rayleigh scattering over which the absorption spectrum of a metal NP is usually superposed. Rayleigh scattering theory addresses the scattering of light by particles whose sizes are much smaller than the wavelength of the incident light (wavelength > π * particle size). When a photon is scattered by a NP, its angle of propagation changes while its frequency stays the same. The intensity of the scattered light I_s is inversely proportional to the fourth power of the wavelength.

Now that we have introduced the theory describing the effect of an incident light impinging on metallic NPs, we may study the interaction of the NPs with fluorescent dye molecules.

2.2 Plasmon-Dye Interactions

Metal NPs and other metallic nanostructures can increase the fluorescence intensity of fluorescent dye molecules located in their proximity. Two distinct mechanisms have been proposed in order to explain the enhancement of the optical properties of these fluorophores placed in close proximity to metallic NPs. The first is energy transfer between the dye molecules and the metal NPs, resulting either in surface enhanced fluorescence or surface enhanced absorption of the dye molecules. In order to obtain an effective energy transfer, the SPR peak of the NPs can be tuned by monitoring the physical dimensions and composition of the particles. The second mechanism that can result in surface enhancement of the fluorescence of the dye molecules is the decrease of their radiative and non radiative lifetimes due to the coupling of the dye dipole moment with the electric field induced by the surface plasmon polaritons [44]. Indeed, when light is coupled as a surface plasmon in a metal NP, it induces an evanescent electromagnetic field coming out of the surface of the NP and decaying into the surrounding dielectric field [42d]. The distance between the dye molecule and the particle is crucial in both mechanisms.

2.2.1 *Energy Transfer*

When a dye molecule is located in the vicinity of a metal surface, the energy levels of the dye and the surface plasmon may couple, resulting in energy transfer between them. Depending on the nature of the coupling, the effect of this energy transfer may be observed as an increase in the dye's absorption coefficient or fluorescence efficiency (see Figure 2.2).

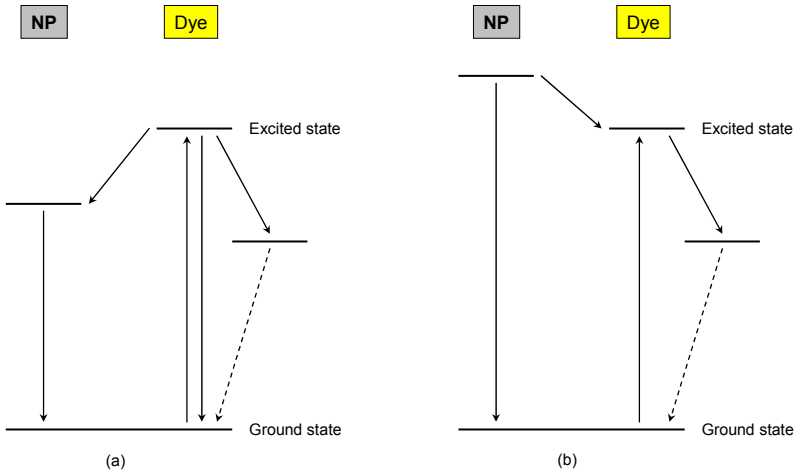

Figure 2.2. Energy diagrams describing surface plasmon polariton-dye interaction. (a) Surface enhanced absorption. (b) Surface enhanced fluorescence. The dye's radiative transition is identified with a dashed line. Adapted from [44].

The interaction between light, dyes and NPs can result in two different scenarios (see Figures 2.2a and 2.2b, respectively):

a) The metal NP acts as a reservoir, which can receive the energy from the dye molecule in the excited state. Therefore, the fluorescence of the excited dye molecule is quenched when the energy of the excited dye molecule is transferred to the NP to excite a surface plasmon polariton. As a result, fewer dye molecules are available to return to their ground state through the radiative path (dashed line). Moreover, the dye molecule rapidly drops back to its ground state. Hence, the population of ground state dye molecules that may absorb additional photons is increased, resulting in the enhancement of the absorption of the dye.

b) The dye molecule is excited by a photon or through the transfer of energy from the optically excited surface plasmon polariton. When the metal transfers its energy to the fluorophore, an enhancement of fluorescence is expected due to the higher absorption cross-section of the metal compared to that of the dye molecule.

Two resonance conditions exist: one in which the energy level of the surface plasmon is equal to that of the upper energy level of the excited dye molecule (see Figure 2.3a) and the other in which the energy level of the surface plasmon is equal to that of the radiative transition of the dye molecule (see Figure 2.3b).

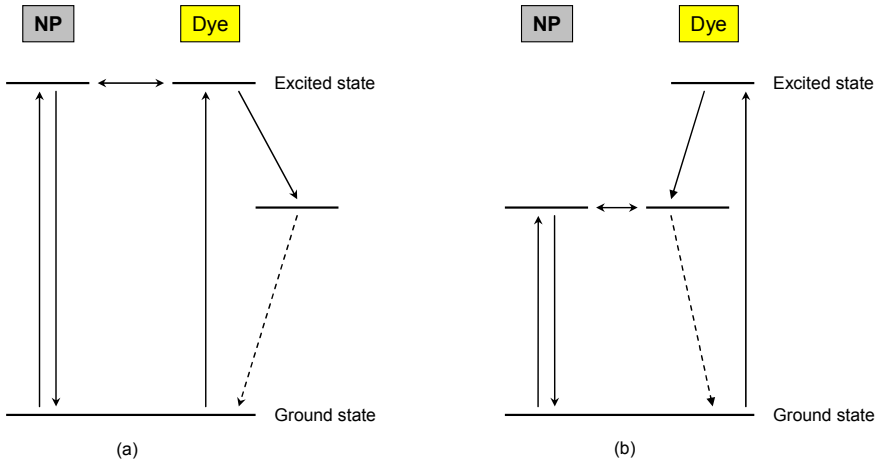

Figure 2.3. Energy transfer resonance conditions. The dye's radiative transition is identified with a dashed line. Adapted from [44].

In the first resonance condition (Figure 2.3a), the energy transfer can either go from the excited surface plasmon polaritons to the dye molecule in the ground state, causing surface enhanced fluorescence, or can originate from the excited dye molecule in order to excite a surface plasmon polariton, causing surface enhanced absorption and quenching of fluorescence. The question as to which process dominates depends on the lifetimes of the surface plasmon polariton and excited dye molecule. The lifetime of the excited dye molecule decreases in the presence of a metallic NP. The magnitude of the reduction is based on the dimensions and composition of the NP and the spatial separation between the dye molecule and the NP [45]. The lifetime of the surface plasmon polariton in gold and silver thin films has been measured and falls between 25 and 800 fs, depending on the morphology of the film [44]. As far as we know, data about the lifetime of surface plasmon polaritons in either gold or silver NPs is not available.

The second resonance condition (Figure 2.3b) usually leads to a quenching of the fluorescence of the dye since the energy transfer generally originates from the excited dye molecules located in the intermediate energy level. The energy transfer process is much localized as the maximum distance separating the dye molecule from the metal NP needs to be between 10 and 30 nm. Quenching decreases with the cube of the distance (d) between the metal surface and the fluorophore molecule [46].

2.2.2 *Electric Field Effects*

As mentioned earlier, light can couple into a metal NP, giving rise to a localized surface plasmon. This localized surface plasmon induces an electric field which has a very high intensity near the surface of the NP, and decays as the distance is increased away from the surface of the particle. Hence, there is a confinement of electromagnetic radiation around the metallic nanostructure. This electric field enhancement is wavelength-dependent. Large particles give smaller enhancement, with a shift of the plasmon resonance to longer wavelengths [42c].

When a dye molecule is within the extended electric field of a surface plasmon, the radiative decay rate of the dye can increase. The manipulation of the radiative decay properties of a fluorescent molecule is sometimes referred to as radiative decay engineering [12]. To understand the importance of controlling the radiative decay rate, it is necessary to study how this rate influences the quantum yield Q_0 and lifetime τ_0 of a dye molecule in the absence of a metal surface. The quantum yield and lifetime in the absence of other quenching interaction are given respectively by:

$$Q_0 = \frac{\Gamma}{\Gamma + k_{\mathrm{nr}}} \quad (2.5)$$

$$\tau_0 = \frac{1}{\Gamma + k_{\mathrm{nr}}} \quad (2.6)$$

where Γ is the radiative decay rate, and k_{nr} is the nonradiative decay rate [12]. The natural or radiative lifetime of a fluorophore (τ_N) is the inverse of the radiative decay rate ($\tau_N = \Gamma^{-1}$). It is the lifetime that would be observed if the quantum efficiency of the fluorophore were equal to one ($k_{\mathrm{nr}} = 0$). The quantum yield relates to the fraction of excited fluorophores that undergo a radiative transition (Γ) to the ground state compared to the total decay ($\Gamma + k_{nr}$). As stated in equation 2.6, the lifetime of an excite dye molecule is equal to the inverse sum of the rates (radiative and nonradiative) that reduce the population of dye molecules in the excited state. Fluorescent molecules with high radiative rates have high quantum efficiencies and short lifetimes. The radiative rates are determined by the extinction coefficients of the fluorophores, which are slightly dependent of the surrounding medium. Thus, the radiative decay rate can be considered

invariable for any given fluorophore. As a result, the quantum efficiency may be increased by decreasing the nonradiative rate k_{nr}, which can be achieved by lowering the temperature. The lifetime of a fluorescent dye may be increased or decreased by varying the nonradiative decay rate k_{nr}. For a given change in $k_{nr,}$ the lifetime and quantum yield of a fluorophore increase or decrease together [12]. Collisional quenching (used to characterize collisions between biomolecules and fluorophores) with a biomolecular rate constant k_q can decrease the quantum yield and the lifetime of a fluorophore by addition of a nonradiative transition to the ground state, k_q $[Qu]$, where $[Qu]$ is the quencher concentration. This is described by the following relations:

$$Q = \frac{\Gamma}{\Gamma + k_{nr} + k_q[Qu]} \quad (2.7)$$

and

$$\tau = \frac{1}{\Gamma + k_{nr} + k_q[Qu]} \quad (2.8)$$

The quantum yield and lifetime of a fluorophore can also be modified by the addition of a resonance energy transfer rate process, k_T, which depopulates the excited state. The quantum efficiency and lifetime become:

$$Q = \frac{\Gamma}{\Gamma + k_{nr} + k_T} \quad (2.9)$$

and

$$\tau = \frac{1}{\Gamma + k_{nr} + k_T} \quad (2.10)$$

Usually the only way to alter the value of the quantum yield and lifetime of a fluorophore is by changing k_{nr}, k_q $[Qu]$, and k_T [12].

However, the presence of a nearby metal can increase the radiative rate by addition of a new radiative channel Γ_m (the quenching caused by the metal will not be considered for the purpose of the discussion). The quantum yield and lifetime of the dye are thus given by:

$$Q_{\mathrm{m}} = \frac{\Gamma + \Gamma_{\mathrm{m}}}{\Gamma + \Gamma_{\mathrm{m}} + k_{\mathrm{nr}}} \quad (2.11)$$

and

$$\tau_{\mathrm{m}} = \frac{1}{\Gamma + \Gamma_{\mathrm{m}} + k_{\mathrm{nr}}} \quad (2.12)$$

The increment in the value of Γ_{m} causes the quantum yield to increase and the lifetime to decrease. It is of interest to consider the effect of radiative rate enhancement for high and low intrinsic quantum yield fluorophores. If the dye has a high quantum yield ($Q_0 \rightarrow 1$), then the additional radiative channel has almost no effect on the quantum yield, and energy transfer quenching to the metal will need to be considered. If the dye has a low quantum yield or is nearly "nonfluorescent", then the additional radiative decay rate will substantially increase the quantum yield [12].

A further understanding of radiative decay rate requires one to take a look at the microscopic theory of radiative transition. The metallic NP can act as a mirror in the proximity of a fluorophore, thereby causing the emitted photon from the dye to bounce back. Hence, a larger number of photons interact with the dye molecules, forcing them to drop back to the ground state by stimulated emission. The probability that the dye molecules will make a stimulated jump to the ground state is described by the quantum mechanical transition probability per unit time, W_{ij}, which according to Fermi's Golden Rule is given as follows:

$$W_{ij} = \frac{2\pi}{h}\left|\mu_{ij}\right|^2 \rho\left(\nu_{ij}\right) \quad (2.13)$$

where h is Planck's constant, μ_{ij} is the transition dipole moment connecting the initial state, i, and the final state, j; and $\rho(\nu_{ij})$ is the photon mode density at transition frequency ν_{ij} corresponding to the energy gap between the initial and the final states. It is the density term $\rho(\nu_{ij})$, which may be increased by placing a metal NP in close proximity of a dye molecule [42e]. This process is more effective when the fluorophore is placed in close proximity to metal flat surfaces like metal thin films.

We can summarize the interactions between a fluorescent dye and a metallic surface by three major effects: quenching of fluorescence, local field enhancement, and enhancement of the radiative decay rate. The combined action of all these effects may be described by an apparent quantum yield Y, which relates to the fluorescence intensity of the dye samples in the presence of metal NPs to the control samples (without the particles), measured with the same intensity of incident light.. While the true quantum yield cannot be greater than one, the apparent quantum yield refers to the impact of local field enhancement, and can be larger than one. It is given as:

$$Y = \left|L\left(\omega_{em}\right)\right|^2 Q_m \quad (2.14)$$

where Q_m is the net quantum yield given by equation 2.11, and $L(\omega_{em})$ refers to the local field enhancement at the emission frequency ω_{em} [42f]. $L(\omega_{em})$ is proportional to the product of the quantum yield without metal and the amplification of the incident field. Therefore, metal particles can be at the origin of greatly enhanced local excitation intensities since the light intensity is proportional to the square of the electric field [12]. If the local field $L(\omega_{em})$ is substantially enhanced (*i.e.* Γ_m is significantly larger than k_{nr}) the quantum yield is increased and the lifetime is decreased. When the value of k_{nr} is significantly larger than the value of Γ_m due to metal induced-quenching, both the quantum yield and lifetime are reduced [42f].

The magnitudes of these three types of interactions mentioned above depend on the location of the fluorophore around the metallic NP and the orientation of its dipole moment with respect to the metallic surface. When the distance separating the fluorophore from the metal surface is less than 5 nm, the metal-induced quenching dominates. For distances between 5 nm and 20 nm, enhancement of fluorescence can be realized [42f]. If the dye molcecule-NP distance is too large (greater than 100 nm), there is little enhancement of fluorescence. It is also important to take into account the aspect ratio of the metallic NP since spheroids with aspect ratios different from 1:1 may lead to larger enhancement of fluorescence signals for certain dye-NP separating distances [44].

3 Materials and Experimental Method

This chapter describes the experimental procedures that were followed in order to further analyze the interaction of NPs with dye molecules. For this research, gold-silver nanoalloys (Au_x-Ag_{1-x} nanoalloys) were synthesized and placed in the vicinity of fluorescent dyes, namely rose bengal, rhodamine B, and fluorescein sodium.

3.1 Generalities

Starting materials included rose bengal, rhodamine B, fluorescein disodium salt hydrate (also known as fluorescein sodium), and hydrogen tetrachloroaurate ($HAuCl_4$), which were purchased from Alfa Aesar. In addition, a 1.0 N silver nitrate ($AgNO_3$) solution and sodium citrate were supplied by Fisher Scientific. Deionized water, which had a resistance of 18.6 MΩ was also used.

Three techniques were used to evaluate the Au_x-Ag_{1-x} nanoalloys: UV-Vis absorption spectroscopy, dynamic light scattering (DLS) and transmission electron microscopy (TEM). Absorption spectra were collected using a Shimadzu UV-3101PC, particle size distributions were measured using a NanoZS model number ZEN 3600, and TEM images were obtained using a Philips EM420T transmission electron microscope. Fluorescence spectroscopy was used to determine the existence of either surface enhanced fluorescence or quenching of fluorescence of the dye molecules mixed with Au_x-Ag_{1-x} nanoalloys. These measurements were carried out using a fluorescence spectrometer that was assembled using a tungsten light source, two Jobin Yvon Spex 1680 monochrometers, and a R928 multi-alkali photomultiplier tube (PMT). The current was fixed at 10 A rather than the maximum rated current, which meant that the power dissipated by the lamp was 200W. Slits of various sizes were used at the entrance and exit of each monochrometer in order to control the amount of light which would be received by the sample and the detector. When necessary, two neutral density filters

(optical density = 1) were utilized to prevent the saturation of the PMT. Two types of measurement were performed: fluorescence and photoluminescence excitation spectroscopy. In the fluorescence measurement, the fluorescence signal was obtained by exciting the sample with a specific pump wavelength, selected by setting the grating angle of the monochrometer between the tungsten lamp and the sample, and measuring the fluorescence intensity within a specific wavelength range while scanning the monochrometer positioned between the sample and the PMT. For photoluminescence excitation spectroscopy, the wavelength monitored by the PMT was fixed by setting the grating angle of the monochrometer between the sample and the PMT, and the excitation spectrum was measured within a specified wavelength range while scanning the monochrometer positioned between the lamp and the sample. An iterative process between these two measurement techniques was used to determine the optical pump wavelength needed to obtain the maximum fluorescence signal. For absorption and fluorescence measurements, sample solutions were analyzed in 3.5 mL polystyrene four-sided square cuvettes with an optical path length of 1 cm. Two replicates of each fluorescence and photoluminescence excitation measurement were performed for each experiment.

3.2 Synthesis of Au_x-Ag_{1-x} Nanoalloys

Stock solutions of 2.0 mM $HAuCl_4$, 2.0 mM $AgNO_3$, and 6.0 mM sodium citrate were initially prepared by mixing an appropriate amount of these products with deionized water. The NPs synthesis was based on a study published by El-Sayed *et al*. [47]. A matrix of four nanoalloys stock solutions ($Au_{1.00}$-$Ag_{0.00}$, $Au_{0.75}$-$Ag_{0.25}$, $Au_{0.5}$-$Ag_{0.5}$, $Au_{0.25}$-$Ag_{0.75}$), each with a specific fraction of gold and silver, was obtained by reducing $HAuCl_4$ and $AgNO_3$ with sodium citrate. These particles were synthesized while heating the mixture to 100 ˚C for 30 minutes. For all stock solutions of NPs, the total concentration of gold and silver reactants was 0.20 mM, and the concentration of sodium citrate was 2.0 mM. There was no evidence that silver NPs formed when only $AgNO_3$ and sodium citrate were present in the solution.

3.3 Preparation of Dye Stock Solutions

As mentioned previously, three fluorescent dyes were used for this research: rose bengal, rhodamine B, and fluorescein sodium. Three 20 mM stock solutions of these dyes were prepared using a 2.0 mM sodium citrate solution as the solvent to provide a constant background of citrate ions in the dye and dye-nanoparticle solutions.

3.4 Preparation of Dye Control Solutions and Dye-NPs Solutions

Six experimental matrices of dye and dye-NPs were prepared in order to understand how the average dye-NP spacing and the difference in energy between the SPR peak of the NPs and the fluorescence peak of the dye-NPs mixtures affected the fluorescence signal detected from the solutions. The control solutions of dyes contained a fixed concentration of sodium citrate (2.0 mM), while the dye concentration was decreased by a factor of 4, from 2.0 mM to 7.8 μM. The dye-NPs solutions had a constant concentration of NPs (0.20 mM) whereas the dye concentration was also decreased by a factor of 4, from 2.0 mM to 7.8 μM.

4 Results and Discussion

This chapter presents and discusses the optical characterization of Au_x-Ag_{1-x} nanoalloys and analyzes the interaction of the NPs with three fluorescent dye molecules: rose bengal, rhodamine B, and fluorescein.

4.1 Characterization of Au_x-Ag_{1-x} Nanoalloys

Gold and silver ions were reduced simultaneously by sodium citrate in the same solution to form gold-silver nanoalloys. The optical absorption spectrum of such alloys showed only one plasmon band [48, 49]. Since the simple mixture of gold and silver NPs would cause two plasmon bands, a single band was a proof for the formation of gold-silver nanoalloys.

Figure 4.1 shows the optical absorbance data for gold and several gold-silver alloy NPs with varying gold and silver proportions. When analyzing the absorption data, it was assumed that the visible absorption of an aqueous solution of gold NPs and gold-silver alloy NPs was a result of a linear combination of losses due to Rayleigh scattering and losses due to the excitation of the surface plasmons. As mentioned in 2.1, Rayleigh scattering has a strong dependence on the wavelength of light, since the intensity of the scattered light is inversely proportional to λ^4. The scattered irradiance I_s approximated by C / λ^4, where C is a constant, was subtracted from the absorbance curves collected, leaving the absorbance caused by the excitation of the surface plasmons in the NPs. A small baseline offset, associated with a drift in the electronics of the spectrophotometer and which was independent of the wavelength, was also subtracted from the data. The resulting spectra was analyzed to determine the peak wavelength and the full width half maximum (FWHM) of the SPR peak.

The varying ratios of gold and silver produced solutions of Au_x-Ag_{1-x} nanoalloy colloids which had SPR wavelengths between that of gold (~ 525 nm) and that of silver

(~ 425 nm). Specifically, the plasmon band blue shifted with an increasing amount of silver, from 525 nm to 442 nm. The theoretical FWHM of the SPR peak for a monodispersed solution of spherical gold NPs with a 20 nm diameter in pure water at room temperature is about 55 nm wide. Therefore, the FWHM revealed that the colloidal solutions of gold NPs (FWHM ≈ 84 nm) and $Au_{0.25}$-$Ag_{0.75}$ nanoalloys (FWHM ≈ 70 nm) were fairly monodispersed. Nevertheless, the very broad SPR peaks of $Au_{0.50}$-$Ag_{0.50}$ (FWHM = 218 nm) and $Au_{0.75}$-$Ag_{0.25}$ (FWHM = 172 nm) alloy NPs were an indication of polydispersed solutions or solutions of non spherical NPs. TEM micrographs (see Figure 4.3) and DLS data were collected in order to confirm these observations.

There was a small size distribution of the 100% gold NPs (DLS revealed an average diameter of about 12 nm, with a size distribution of 17%), which were mostly spherical in shape. This observation was reasonable, given the small FWHM of the SPR peak associated with these particles.

While there is some aggregation of the $Au_{0.75}$-$Ag_{0.25}$ alloy NPs, the aggregates themselves are considerably smaller and more regular in shape than these observed for the $Au_{0.50}$-$Ag_{0.50}$ nanoalloys. This explains the broader FWHM of the $Au_{0.50}$-$Ag_{0.50}$ alloy NPs compared to that of the $Au_{0.75}$-$Ag_{0.25}$ particles. Lastly, in spite of the larger size (roughly 50 nm) of the $Au_{0.25}$-$Ag_{0.75}$ particles, they were fairly spherical in shape, with a small size distribution which was expected given the narrow FWHM of the SPR curve. Two distinct populations of NPs were found for $Au_{0.50}Ag_{0.50}$ and $Au_{0.25}$-$Ag_{0.75}$ (see Figures 4.3c and 4.3d). The larger diameters were on the order of 200 nm (due to the aggregation of smaller size NPs) in Figure 3C, and 50 nm in Figure 3D. The second set of NPs are extremely small (2 nm or smaller in diameter) and spherical in shape. We speculated that these smaller NPs were composed of pure silver, rather than a gold-silver alloy. The presence of these two populations of NPs resulted in the very broad SPR peak in the absorption spectrum of the $Au_{0.50}$-$Ag_{0.50}$ alloy NPs, and in the short wavelength tail in the absorption spectrum of the $Au_{0.25}$-$Ag_{0.75}$ particles (see Figure 4.2). The presence of these very small NPs was not observed in the DLS data on the Au_x-Ag_{1-x} colloids, as their diameter was below the detection limit of the instrument.

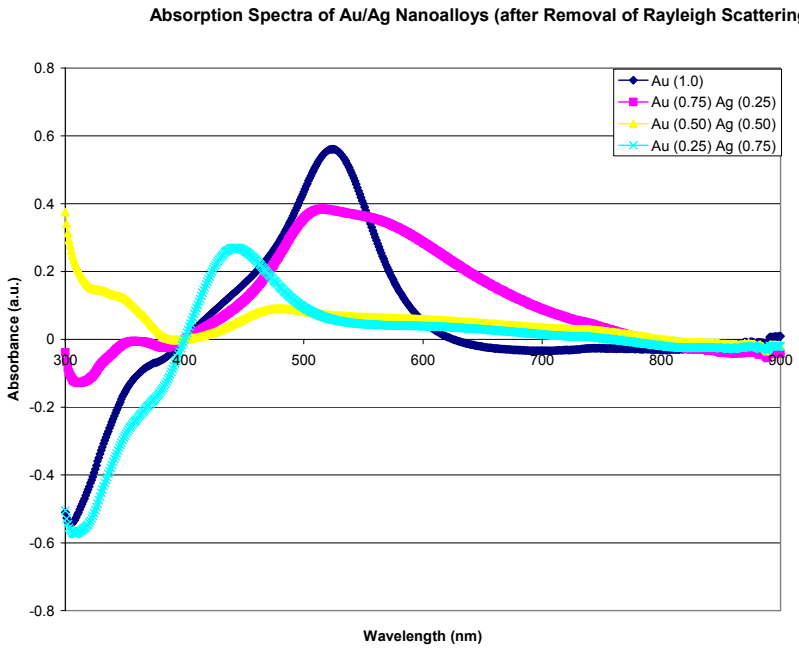

Figure 4.1. Absorption spectra of Au_x-Ag_{1-x} NPs, where x = 1.0, 0.75, 0.50, and 0.25. The reaction temperature was 100 ˚C.

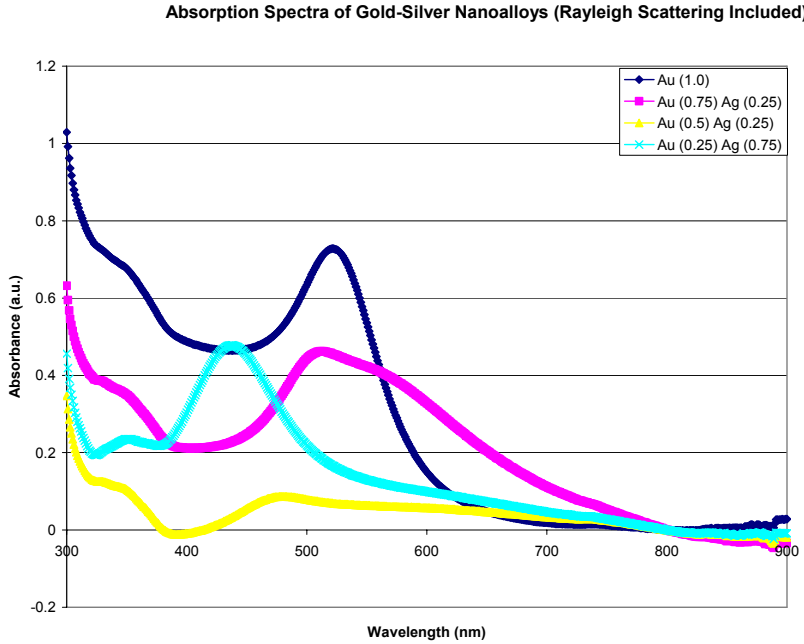

Figure 4.2. Absorption spectra (Rayleigh scattering included) of Au_x-Ag_{1-x} NPs, where x = 1.0, 0.75, 0.50, and 0.25. The reaction temperature was 100 ˚C.

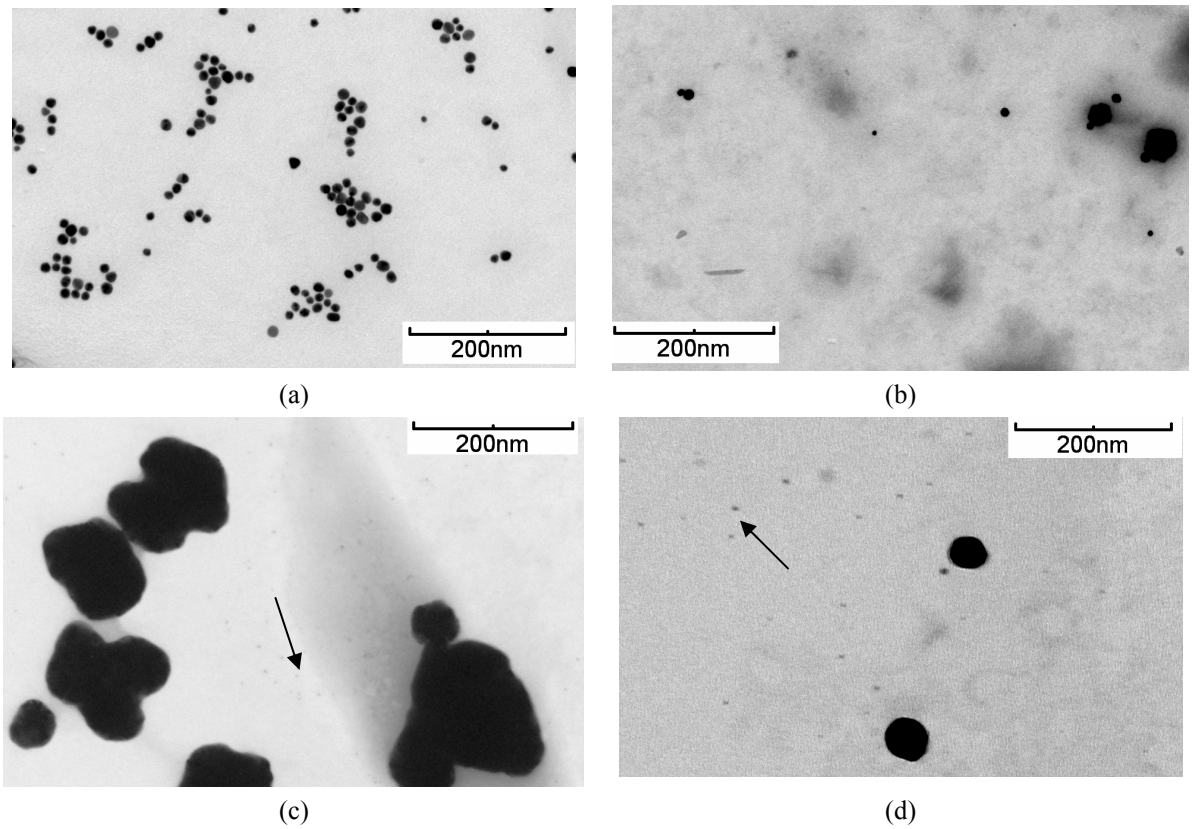

(a) (b)

(c) (d)

Figure 4.3. TEM images of (a) 100% Au, (b) $Au_{0.75}$-$Ag_{0.25}$, (c) $Au_{0.50}$-$Ag_{0.50}$, and (d) $Au_{0.25}$-$Ag_{0.75}$ NPs. Arrows in (c) and (d) mark the location of very small NPs. Photographed by author and William C. Miles.

4.2 Fluorescence Analysis of Fluorophore-NPs Solutions

Three fluorescent dyes, namely rose bengal, rhodamine B, and fluorescein sodium were studied in the presence of NPs (see Figure 4.4 for the respective Lewis formulas). Rose bengal and rhodamine B were chosen as they exhibit almost similar emission wavelengths (approximately 570 nm) but have very different quantum yields (2% for rose Bengal [50] and 31 – 48% for rhodamine B [50,51] in water). Fluorescein is a common dye used in biological sensing. Its fluorescence wavelength is shorter than that of rose Bengal and rhodamine B (~525 nm) but is quantum yield reaches 95% in water [51].

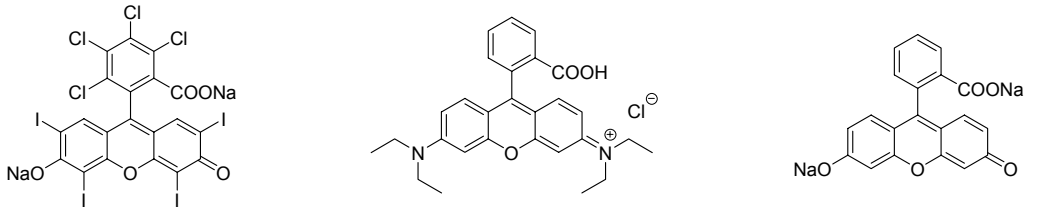

Figure 4.4. Chemical structures of (a) Rose Bengal; (b) Rhodamine B; (c) Fluorescein sodium.

In order to study these dye-NP systems, absorption, excitation and fluorescence spectra were collected. However, a number of absorption spectra were not useful due to the extremely low intensity of light that passed though the samples, even when the optical path was reduced to 1 mm. The opacity of these mentioned samples was due to a high concentration of fluorophore and possibly to a surface enhancement of the dye's absorbance. Therefore, the absorption data could not be used to determine whether the absorption of the dye molecules was enhanced in the presence of NPs.

DLS measurements were also performed in order to determine an approximate number of NPs per milliliter of solution according to the relation:

$$N = \frac{6C}{\pi d^3 \rho} \quad (4.1)$$

where C (g/cm^3) is the total NPs concentration in the solution, d (cm) is the particle diameter, and ρ (g/cm^3) is the NP density [52]. The use of this equation required the assumption that all of the $HAuCl_4$ and $AgNO_3$ were utilized in the formation of Au_x-Ag_{1-x} alloy NPs. Moreover, it was necessary to assume that gold and silver densities, which were well known for their bulk state, were the same in their quantized state.

The presence of very small NPs (2 nm or less in diameter) was not observed in the DLS data on the Au_x-Ag_{1-x} colloids ($x \leq 0.5$) as their diameter was below the detection limit of the instrument. In addition, the diameters of the NPs given by the DLS instrument were not their true diameters, but merely their hydrodynamic diameters. The gold and silver atoms, which have clouds of electrons in their conduction band, attracted hydrogen ions from the water and citrate ions from the sodium citrate, causing a grading of the refractive index of water from the solution to the metal NP interface. This effect

resulted in measurements of larger diameters than their actual values for these metal NPs. Hence, the concentrations of nanoalloys calculated using the DLS data underestimated the actual concentrations.

Equation (4.1) was transformed in order to include the number percentage of each diameter NP, according to the relation:

$$N = \frac{6C}{\pi\rho\sum_i d_i^3 \alpha_i} \quad (4.2)$$

where C (g/cm^3) is the solution concentration, ρ (g/cm^3) is the NP density, d_i is the particle diameter and α_i is the corresponding percentage of this particle in solution. When dealing with alloy NPs, equation (4.2) became:

$$N = \frac{6}{\pi\sum_i d_i^3 \alpha_i}.\left(\frac{C_{Au}}{\rho_{Au}} + \frac{C_{Ag}}{\rho_{Ag}}\right) \quad (4.3)$$

where C_{Au} and C_{Ag} are respectively the gold and silver concentrations in solution, and ρ_{Au} and ρ_{Ag} respectively the gold and silver densities. From equation (4.2), the approximate distance x [nm] between NPs and fluorescent dye molecules was derived:

$$x = 10^8.\sqrt[3]{\frac{1}{N_A.c_d}} \quad (4.4)$$

where c_d is the concentration of fluorescent dye in the NP/dye mixture [mol/L] and N_A the Avogadro's number.

4.2.1 *Rose Bengal / NPs Interactions*

Figure 4.5 shows that the peak of the fluorescence signal moved to longer wavelengths as the dye concentration increased in the presence of NPs. This red shift was globally the same for all combinations of gold and silver NPs compared to the control solutions of rose bengal. However, this shift appeared to be the largest when the sample contained $Au_{0.5}$-$Ag_{0.5}$ NPs. This red shift could be a result of absorption of the

fluorescence of the dye molecules, particularly at short wavelengths where the energy of the emitted photons overlap the SPR peak of the metallic NPs.

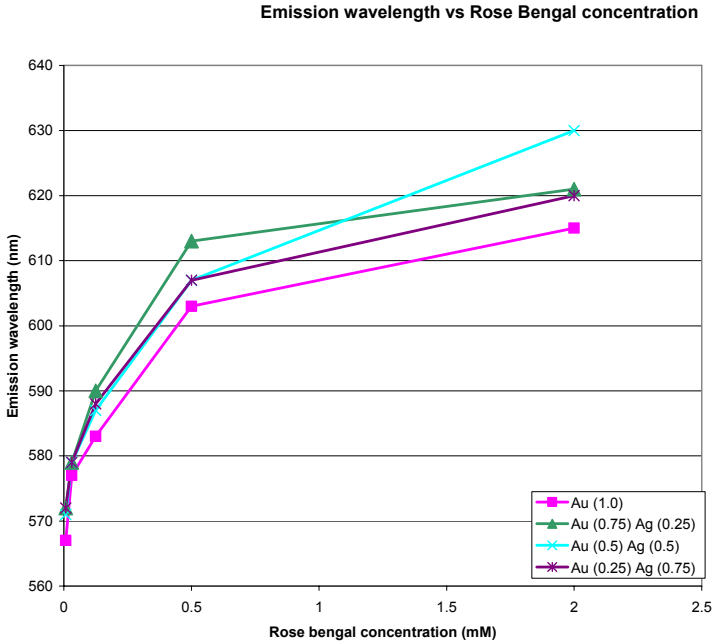

Figure 4.5. Peak emission wavelength of rose bengal as a function of dye concentration with 0.2 mM of $Au_{1.0}$-$Ag_{0.00}$ (pink), $Au_{0.75}$-$Ag_{0.25}$ (green), $Au_{0.50}$-$Ag_{0.50}$ (blue), and $Au_{0.25}$-$Ag_{0.75}$ (purple).

For a particular concentration of rose bengal in solution, a ratio of the peak intensity of the fluorescence signal of the dye-NP solution to the peak intensity of the fluorescence signal of the dye solution was computed in order to determine whether surface enhanced fluorescence or quenching occurred. When the ratio was greater than 1, the fluorescence signal from the dye-NP solutions was larger than that of the dye solution as a result of surface enhancement. When the ratio was less than 1, the fluorescence signal from the dye-NPs was smaller than that of the dye solution because the energy of the excited dye molecules was transferred to the NPs and the fluorescence signal was quenched.

This ratio was plotted as a function of the concentration of rose bengal in the solution (see Figure 4.6). Based on the theory described in 2.2.2, an enhancement in fluorescence intensity was expected since the intrinsic quantum efficiency of rose bengal is very low. The greatest fluorescence enhancement occurred at the highest concentration

(2.0 mM) of rose bengal in the presence of $Au_{0.75}$-$Ag_{0.25}$ or $Au_{0.25}$-$Ag_{0.75}$ (enhancement factor around 5).

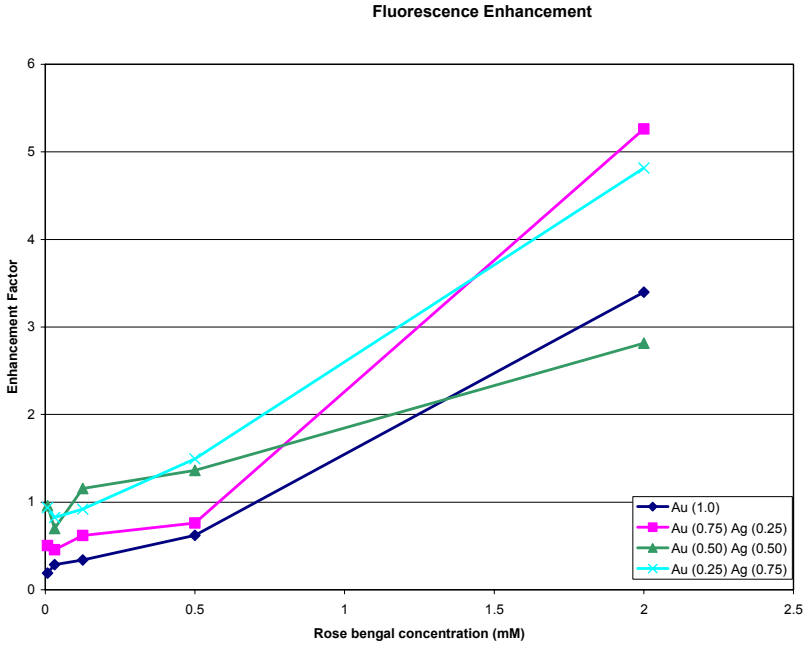

Figure 4.6. Ratio of the peak fluorescence signal of rose bengal-NP solutions to rose bengal solutions, as a function of the concentration of rose bengal in solution. A ratio greater than 1 indicated surface enhanced fluorescence and a ratio less than 1 fluorescence quenching, when the NPs were in solution with rose bengal.

The concentration of NPs and dye molecules in the solution were subsequently used to estimate the average dye-NP spacing. Surface enhanced fluorescence was observed in all dye-NP solutions when the average distance between the dye molecules and NPs was between 9 and 15 nm. This distance was slightly shorter than that predicted by theory (between 10 and 30 nm), but was still remarkably accurate, considering the simplicity and the level of approximation of the model (see Figure 4.7).

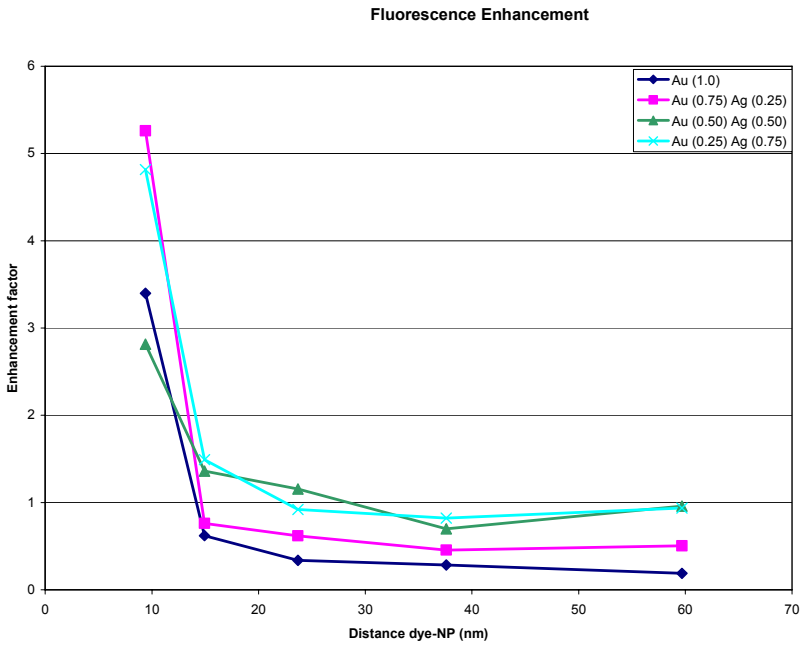

Figure 4.7. Ratio of the peak fluorescence signal of rose bengal-NP solutions to rose bengal solutions as a function of the average separation between the dye molecules and NPs.

We note that quenching of the fluorescence was observed when there were supposed to be large distances between the nanoparticles and rose bengal molecules. This is contrary to the theory presented in Chapter 2.2, where it was noted that little enhancement or quenching of the dye fluorescence should occur when the distance between the metallic nanoparticle and dye molecule is greater than 30-100nm. Quenching of the dye's fluorescence is only expected when the distance between the nanoparticle and dye molecule is small enough to permit energy transfer between them, less than 10 nm. For this reason, we speculate that there was a possibility of adsorption of the dye molecules to the NP surface. The NPs used in these fluorescence measurements were uncoated. Gold and silver have a high concentration of nearly free electrons on their surface, which can interact with charges on the rose bengal molecule (the negatively charged carboxylate function, for example – see Figure 4.4a) and may cause the rose bengal molecules to be attracted to the metal nanoparticles' surface. In this case, the fluorescence quenching that was observed at low concentrations of dye molecules might be a result of energy transfer from the excited dye molecule to the metal NP – a process that can occur efficiently when there is a very small distance (< 10 nm)

between the dye molecule and the NPs. As the dye concentration was increased, the loading of the dye on the surface of the NPs might have increased until saturation of the surface of the NP. At dye concentration greater than this point, surface enhanced fluorescence would be possible; resulting from a decrease in the radiative lifetime of the excited dye molecules caused by the interaction of the electric field induced by the surface plasmons with the dye molecules. Unfortunately, there is no way to verify if adsorption of the dye molecules on the NPs occurred with the measurements performed during this research project.

4.2.2 *Rhodamine B / NPs Interactions*

The same matrix of experiments was performed with rhodamine B. As mentioned earlier, the fluorescence wavelengths of rhodamine B and rose bengal are almost identical (within 10 nm). Contrary to rose bengal (quantum yield of 2%), rhodamine B can be classified as a strong dye as its quantum yield is about 48%. Therefore, according to the theory discussed in 2.2.2, an insignificant fluorescence enhancement was expected using all four types of nanoalloys ($Au_{1.0}$-$Ag_{0.00}$, $Au_{0.75}$-$Ag_{0.25}$, $Au_{0.50}$-$Ag_{0.50}$, and $Au_{0.25}$-$Ag_{0.75}$).

The emission wavelength was plotted as a function of dye concentration (see Figure 4.8). Here again, the peak of the fluorescence signal moved to longer wavelengths as the dye concentration increased. This red shift was globally the same for all combinations of gold and silver compared to the control solutions of rhodamine B.

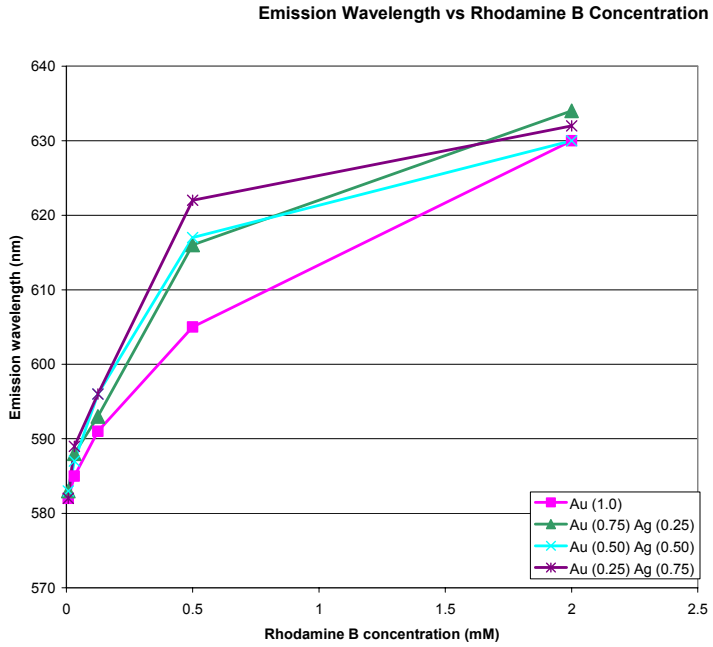

Figure 4.8. Peak emission wavelength of rhodamine B as a function of dye concentration with 0.20 mM of $Au_{1.0}$-$Ag_{0.00}$ (pink), $Au_{0.75}$-$Ag_{0.25}$ (green), $Au_{0.50}$-$Ag_{0.50}$ (blue), and $Au_{0.25}$-$Ag_{0.75}$ (purple).

Again, for a particular concentration of rhodamine B in solution, the ratio of the peak intensity of the fluorescence signal of the dye-NP solution relative to the peak intensity of the fluorescence signal of the dye solution was calculated in order to determine whether surface enhanced fluorescence or quenching occurred (see Figure 4.9 for a plot of this ratio vs. the concentration of rhodamine B).

We noted a slight enhancement of fluorescence at a rhodamine B concentration of 0.13 mM, and with all four types of NPs ($Au_{1.0}$-$Ag_{0.00}$, $Au_{0.75}$-$Ag_{0.25}$, $Au_{0.50}$-$Ag_{0.50}$, and $Au_{0.25}$-$Ag_{0.75}$). Quenching of fluorescence was observed with dye concentrations of 7.8 μM, 0.031 mM, and 0.50 mM. This quenching was also noticed with a rhodamine B concentration of 2.0 mM, except when $Au_{0.50}$-$Ag_{0.50}$ were in solution, in which case the intensity of the fluorescence signal of the fluorophore-NP mixture was nearly the same than the signal emitted by the dye alone.

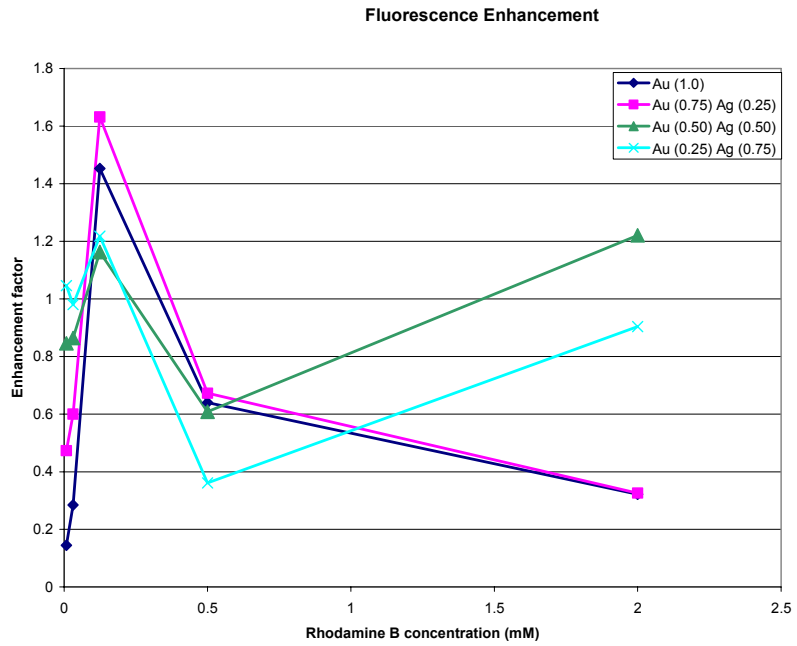

Figure 4.9. Ratio of the peak fluorescence signal of rhodamine B-NP solutions relative to rhodamine B solutions, as a function of the concentration of rhodamine B in solution. A ratio greater than 1 indicated that surface enhanced fluorescence occurred and a ratio less than 1 indicated that fluorescence quenching occurred when the NPs were in solution with rhodamine B.

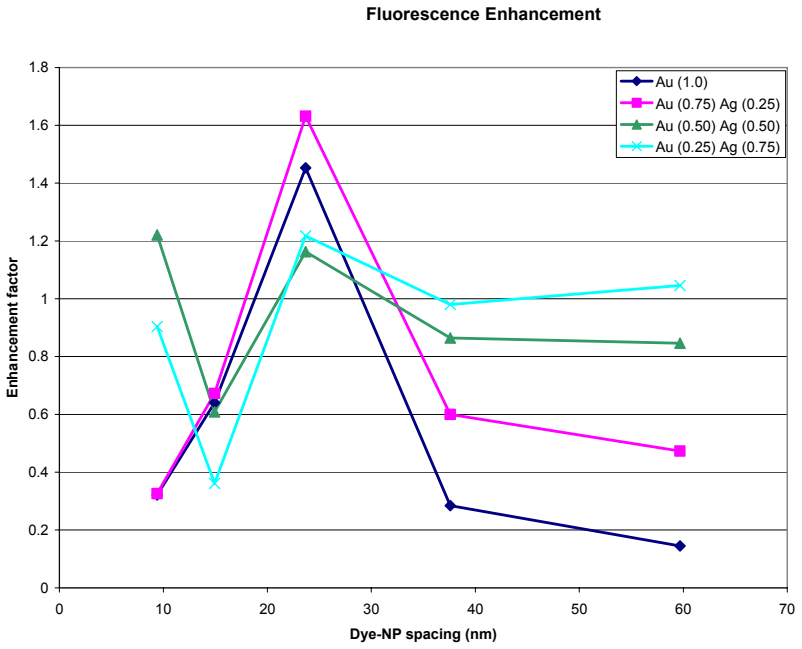

Figure 4.10. Ratio of the peak fluorescence signal of rhodamine B-NP solutions to rhodamine B solutions as a function of the average separation between the dye molecules and NPs.

The enhancement factor was then graphed against the average dye-NP spacing (see Figure 4.10). A slight surface enhanced fluorescence was observed in all dye-NP solutions when the distance separating the dye molecules from the NPs was between 20 and 30 nm, as predicted by theory. Above and below this range, quenching of fluorescence was globally noticed, with the exception of $Au_{0.50}$-$Ag_{0.50}$ NPs. In this case, the enhancement factor had a value of 1.2 for a dye-NP spacing of approximately 10 nm. This result may be an artifact, due to the variability in our measurements.

4.2.3 *Fluorescein Sodium / NPs Interactions*

The same set of experiments was repeated in the presence of fluorescein. The fluorescence wavelength of this dye is shorter than that of rose Bengal and rhodamine B (roughly 525 nm) but its quantum yield reaches 0.95 in water. A near resonance condition was possible when gold NPs are present, similar to that described in Figure 2.3 b. With such a strong dye, we expected fluorescence quenching in all cases (as described in 2.2.2), particularly in the dye-100% Au solutions.

As with the two previous dyes, the peak of the fluorescence signal moved to longer wavelengths as the fluorescein concentration was increased (see Figure 4.11). This red shift was globally the same for all combinations of gold and silver compared to the control solutions of fluorescein.

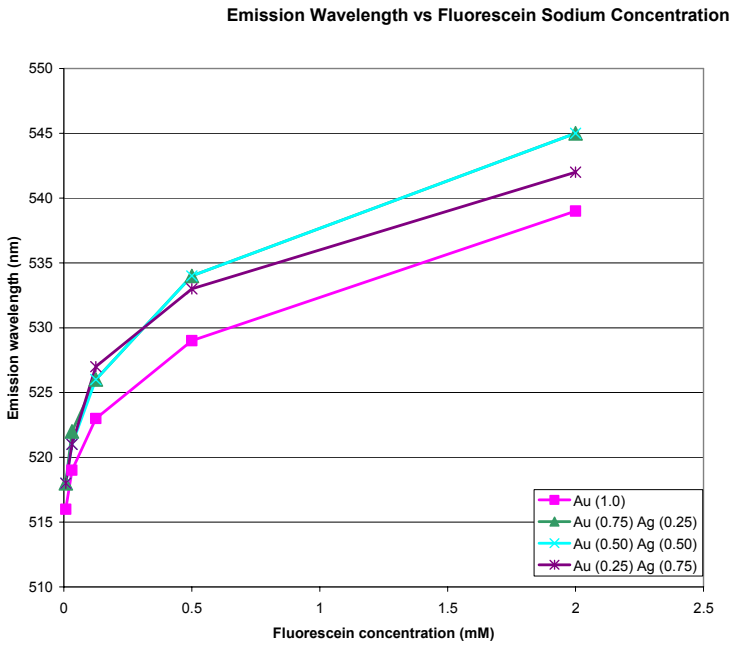

Figure 4.11. Peak emission wavelength of fluorescein as a function of dye concentration without NPs (black line) and with 0.2 mM of $Au_{1.0}$-$Ag_{0.00}$ (pink), $Au_{0.75}$-$Ag_{0.25}$ (green), $Au_{0.50}$-$Ag_{0.50}$ (blue), and $Au_{0.25}$-$Ag_{0.75}$ (purple).

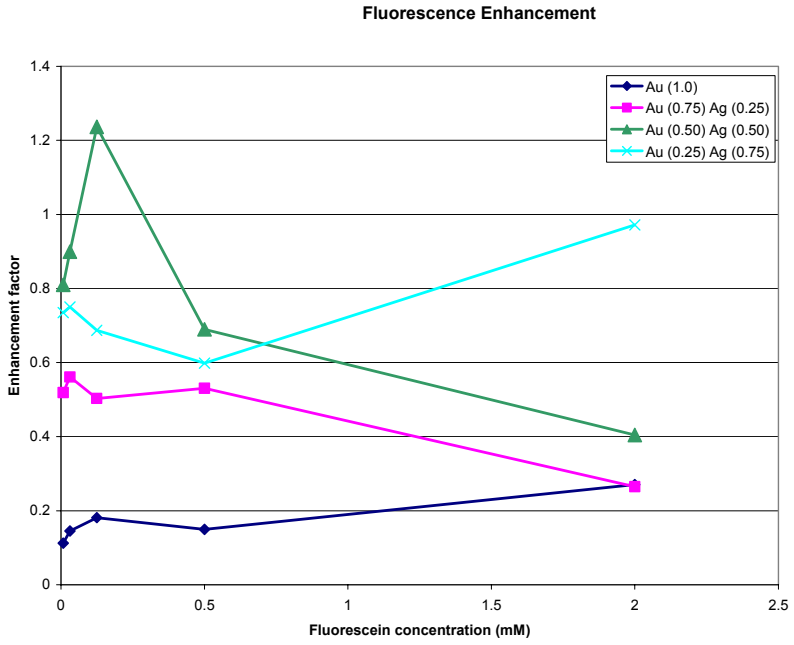

Figure 4.12. Ratio of the peak fluorescence signal of fluorescein-NP solutions relative to fluorescein solutions, as a function of the concentration of fluorescein in solution. A ratio greater than 1 indicated that surface enhanced fluorescence occurred and a ratio less than 1 indicated that fluorescence quenching occurred when the NPs were in solution in the presence of fluorescein.

Fluorescence quenching occurred in almost of all the fluorescein-NP solutions regardless of the dye concentration with considerable quenching observed in the dye-100 % Au solutions. The very slight fluorescence enhancement observed when $Au_{0.50}$-$Ag_{0.50}$ nanoalloys were present in 0.13 mM of fluorescein solution can logically be considered as an artifact due to the variability in our measurements (see Figure 4.12). In Figure 4.13, the enhancement factor was then graphed against the average dye-NP spacing, showing overall quenching (enhancement factor less than 1).

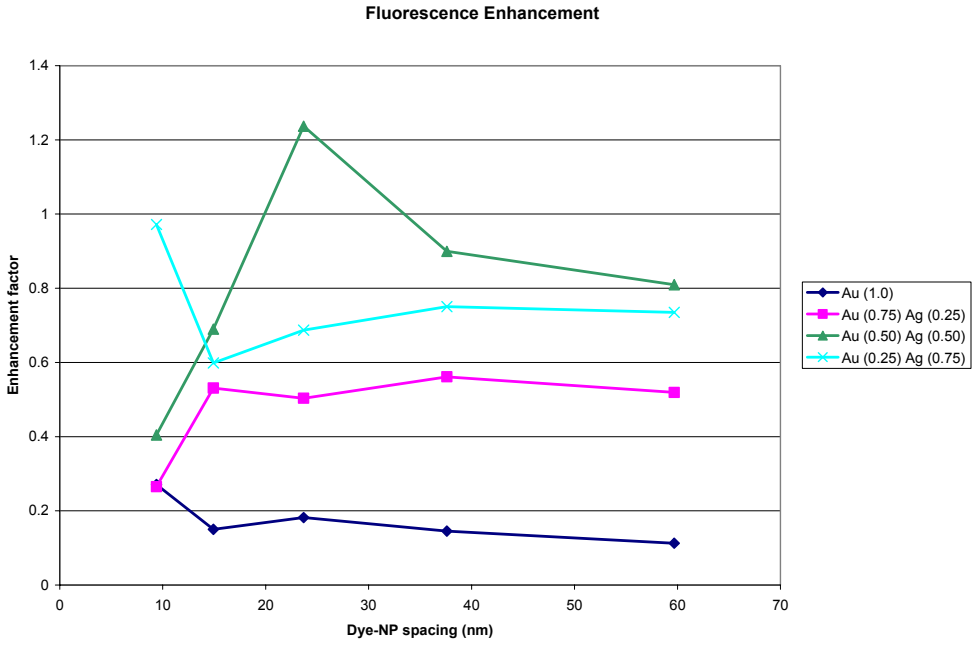

Figure 4.13. Ratio of the peak fluorescence signal of fluorescein-NP solutions to fluorescein solutions as a function of the average separation between the dye molecules and NPs.

4.3 Parameters for Optimum Surface Enhanced Fluorescence

The following table points out the parameters for which highest surface enhanced fluorescence was obtained.

Table 1. Parameters for Optimum Surface Enhanced Fluorescence.

	Rose Bengal	Rhodamine B	Fluorescein
Dye concentration (mM)	2.0	0.13	0.13
Gold-silver ratios	75 : 25	75 : 25	50 : 50
Maximum Fluorescence Enhancement Factor	5.3	1.6	~ 1 [a]
Difference between SPR peak of NP and fluorescence peak of dye molecule (eV)	0.403	0.319	0.242

[a] A very slight fluorescence enhancement (1.2, see Figure 4.12) was observed when $Au_{0.50}$-$Ag_{0.50}$ nanoalloys were present in a 0.13 mM fluorescein solution. However, this can reasonably be considered as an artifact due to the variability in our measurements.

5 Conclusion and Future Work

We have seen that metallic NPs are at the core of very intensive research. They possess the ability to modify the optical properties of fluorescent dye molecules located in their vicinity and, therefore, are investigated for many biosensing applications such as medical imaging, immunoassays, DNA hybridization, and DNA microarrays.

Motivated by the remarkable potential of metal NPs, we conducted our research using gold-silver nanoalloys with varying gold and silver ratios ($Au_{1.00}$-$Ag_{0.00}$, $Au_{0.75}$-$Ag_{0.25}$, $Au_{0.50}$-$Ag_{0.50}$, and $Au_{0.25}$-$Ag_{0.75}$). Optical characterization was performed on these particles utilizing absorption spectroscopy, dynamic light scattering, and transmission electron microscopy. Then, these particles were allowed to interact with three different fluorescent dyes (rose bengal, rhodamine B, and fluorescein sodium) at various concentrations (from 2.0 mM to 7.8 μM). Fluorescence spectra of these mixtures were recorded and analyzed.

A three to five time increase in fluorescence intensity was observed in a 2.0 mM solution of rose bengal with all nanoalloys, a less significant enhancement of fluorescence (1.2 – 1.6 times) was noticed in a 0.13 mM solution of rhodamine B with all four types of NPs, and fluorescence quenching occurred in almost of all the fluorescein-NP solutions regardless of the dye concentration.

The experiments conducted left many questions that were unexplored in the scope of this research. First, it would be beneficial to utilize a method of synthesis that would lead to monodispersed solutions of nanoalloys, since two TEM images have shown aggregates and NPs that were non uniform in size and shape ($Au_{0.75}$-$Ag_{0.25}$ and $Au_{0.50}$-$Ag_{0.50}$). For this purpose, sodium borohydride ($NaBH_4$) could be used as a reducing agent. The formation of very large clusters of $Au_{0.50}$-$Ag_{0.50}$ nanoalloys (~ 200 nm in diameter), and the presence of extremely small NPs in $Au_{0.50}$-$Ag_{0.50}$ and $Au_{0.25}$-$Ag_{0.75}$ also raised many unanswered questions. Therefore, it would be important to better understand the synthesis of gold-silver nanoalloys and its impact on the results obtained.

Prevention of the adsorption of dye molecules on the surface of nanoalloys could also be desirable. This could be achieved by coating the particles with silica which could as well be used to prevent the agglomeration of these NPs. Finally, it would be useful to study the dye-NP interactions by working with dye concentrations larger than 2.0 mM. However, high dye concentrations may lead to new analytical difficulties to overcome saturation of light absorption. Additional experiments using other dyes could be performed in order to show a reliable correlation between the quantum yield of the dye and the fluorescence enhancement in the presence of metallic nanoalloys. While dyes with low quantum yields are expected to display significant fluorescence enhancement under adequate conditions, dyes with high quantum yield should still experience fluorescence quenching.

6 References

[1] M. Kerker, “The optics of colloidal silver: Something old and something new,” *J. Colloid Interface Sci.*, vol. 105, pp. 297–314, Feb. 1985.

[2] D. G. Richards, D. L. McMillin, E. A. Mein, C. D. Nelson, “Gold and its relationship to neurological/glandular conditions,” *Int. J. Neurosci.*, vol. 112, pp. 31– 53, Jan. 2002.

[3] M. Faraday, “The Bakerian lecture. Experimental relations of gold (and other metals) to light,” *Philos. Trans.*, vol. 147, pp. 145–181, Feb. 1857.

[4] E. Hutter, J. H. Fendler, “Exploitation of localized surface plasmon resonance,” *Adv. Mater*., vol. 16, pp. 1685–1706, Oct. 2004.

[5] S. Underwood, P. Mulvaney, “Effect of the solution refractive index on the color of gold colloids,” *Langmuir*, vol. 10, pp. 3427–3430, Jun. 1994.

[6] P. Mulvaney, “Surface plasmon spectroscopy of nanosized metal particles,” *Langmuir*, vol. 12, pp. 788–800, Jul. 1995.

[7] M. C. Daniel, D. Astruc, “Gold nanoparticles: Assembly, supramolecular chemistry, quantum-size-related properties, and applications toward biology, catalysis, and nanotechnology,” *Chem. Rev.*, vol. 104, pp. 293–346, Jan. 2004.

[8] O. Stranik, C. McDonagh, B. D. MacCraith, “Plasmonic enhancement of fluorescence for sensor applications,” in *Photonic Crystal Materials and Nanostructures*, *Proceedings of SPIE*, vol. 5450, R. M. De la Rue, P. Viktorovitch, C. M. Sotomayor Torres, M. Midrio, Eds. Bellingham, WA, 2004, pp. 144–149.

[9] K. L. Kelly, E. Coronado, L. L. Zhao, G. C. Schatz, "The optical properties of metal nanoparticles: The influence of size, shape, and dielectric environment," *J. Phys. Chem. B*, vol. 107, pp. 668–677, Jan. 2003.

[10] C. T. A. Johnk, *Engineering Electromagnetic Fields and Waves.* New York: Wiley, 1975, p. 202.

[11] C. F. Bohren, D. R. Huffman, *Absorption and Scattering of Light by Small Particles*. New York: Wiley, 1983, pp. 82–129.

[12] J. R. Lakowicz, "Radiative decay engineering: Biophysical and biomedical applications," *Anal. Biochem.*, vol. 298, pp. 1–24, Oct. 2001.

[13] K. Aslan, I. Gryczynski, J. Malicka, E. Matveeva, J. R Lakowicz, C. D. Geddes, "Metal-enhanced fluorescence: an emerging tool in biotechnology," *Curr. Opin. Biotech.*, vol. 16, pp. 55–62, Jan. 2005.

[14] A. Kawski, J. Kaminski, E. Kuten, "Quenching of photoluminescence of solutions by electronic excitation transfer," *J. Phys. B: Atom. Molec. Phys*., vol. 4, pp. 609–620, Apr. 1971.

[15] J. R. Lakowicz, J. Malicka, S. D'Auria, I. Gryczynski, "Release of the self-quenching of fluorescence near silver metallic surface," *Anal. Biochem.*, vol. 320, pp. 13–20, Sep. 2003.

[16] J. Malicka, I. Gryczynski, C. D. Geddes, J. R. Lakowicz, "Metal enhanced emission from indocyanine green: a new approach to in vivo imaging," *J. Biomed. Opt.*, vol. 8, pp. 472–478, Jul. 2003.

[17] J. R. Lakowicz, J. Malicka, I. Gryczynski, "Silver particles enhance emission of fluorescent DNA oligomers," *Biotechniques*, vol. 34, pp. 62–68, Jan. 2003.

[18] M. Schena, R. A. Heller, T. P. Theriault, K. Konrad, E. Lachenmeier, R. W. Davis, "Microarrays: Biotechnology's discovery platform for functional genomics," *Trends Biotechnol.*, vol. 16, pp. 301–306, Jul. 1998.

[19] F. Komurian-Pradel, G. Paranhos-Bacala, M. Sodoyer, P. Chevallier, B. Mandrand, V. Lotteau, P. André, "Quantitation of HCV RNA using real-time PCR and fluorimetry," *J. Virol. Methods*, vol. 95, pp. 111–119, Mar. 2001.

[20] N. J. Walker, "A technique whose time has come," *Science*, vol. 296, pp. 557–559, Apr. 2002.

[21] M. J. Difilippantonio, T. Ried, "Technicolor genome analysis," in *Topics in Fluorescence Spectroscopy, DNA Technology*, vol. 7, J. R. Lakowicz, Ed. New York: Kluwer Academic Publishers/Plenum, 2003, pp. 291–316.

[22] J. Malicka, I. Gryczynski, J. R. Lakowicz, "DNA hybridization assays using metal-enhanced fluorescence," *Biochem. Biophys. Res. Commun.*, vol. 306, pp. 213–218, Apr. 2003.

[23] Microarrays : Chipping away at the mysteries of science and medicine. [Online]. Available: http://www.ncbi.nlm.nih.gov/About/primer/microarrays.html.

[24] N. L. W. van Hal, O. Vorst, A. M. M. L. van Houwelingen, E. J. Kok, A. Peijnenburg, A. Aharoni, A. J. van Tunen, J. Keijer, "The application of DNA microarrays in gene expression analysis," *J. Biotechnol,* vol. 78, pp. 271–280, Mar. 2000.

[25] P. O. Brown, D. Botstein, "Exploring the new world of genome with DNA microarrays," *Nat.Genet. Supp.,* vol. 21, pp. 33–37, Jan. 1999.

[26] M. K. Deyholos, D. W. Galbraith, "High-density microarrays for gene expression analysis," *Cytometry,* vol. 43, pp. 229–238, Apr. 2001.

[27] R. J. Lipshutz, S. P. A. Fodor, T. R. Gingeras, D. J. Lockhart, "High density synthetic oligonucleotide arrays," *Nat. Genet. Supp.,* vol. 1, pp. 20–24, Jan. 1999.

[28] DNA microarray. *Wikipedia, the free encyclopedia* [Online]. Available: http://en.wikipedia.org/wiki/DNA_microarray.

[29] J. R. Lakowicz, J. Malicka, I. Gryczynski, "Silver particles enhance emission of fluorescent DNA oligomers," *Biotechniques,* vol. 34, pp. 62–68, Jan. 2003.

[30] W. Rechberger, A. Hohenou, A. Leitner, J. R. Krenn, B. Lamprecht, F. R. Aussenegg, "Optical properties of two interacting gold nanoparticles," *Opt. Commun.,* vol. 220, pp. 137–141, May 2003.

[31] M. K. Oberthaler, T. Pfau, "One-, two-and three-dimensional nanostructures with atom lithography," *J. Phys.: Cond. Matter,* vol. 15, pp. R233–R255, Feb. 2003.

[32] M. P. Zach, R. M. Penner, "Nanocrystalline nickel nanoparticles," *Adv. Materials,* vol. 12, pp. 878–883, June 2000.

[33] N. A. Al-Rawashdeh, M. L. Sandrock, C. J. Seugling, C. A. Foss Jr., "Visible region polarization spectroscopic studies of template-synthesized gold nanoparticles oriented in polyethylene," *J. Phys. Chem. B,* vol. 102, pp. 361–371, Jan. 1998.

[34] J. Malicka, I. Gryczynski, C. D. Geddes, J. R. Lakowicz, "Metal-enhanced emission from indocyanine green: a new approach to *in vivo* imaging," *J. Biomed. Opt.,* vol. 8, pp. 472–478, Jul. 2003.

[35] F. Schutt, J. Fischer, J. Kopitz, F. G. Holz, "Indocyanine green angiography in the presence of subretinal or intraretinal haemorrhages: Clinical and experimental investigations," *Clin. Exp. Ophthalmol.,* vol. 30, pp. 110–114, Feb. 2002.

[36] J. M. Still, E. J. Law, K. G. Klavuhn, T. C. Island, J. Z. Holtz, "Diagnosis of burn depth using laser-induced indocyanine green fluorescence: A preliminary clinical trial," *Burns,* vol. 27, pp. 364–371, Jun. 2001.

[37] R. Boushel, H. Langberg, J. Olesen, M. Nowak, L. Simonsen, J. Bulow, M. Kjaer, "Regional blood flow during exercise in humans measured by near-infrared spectroscopy and indocyanine green," *J. Appl. Physiol.,* vol. 89, pp. 1868–1878, Nov. 2000.

[38] A. Becker, B. Riefke, B. Ebert, U. Sukowski, H. Rinneberg, W. Semmier, K. Licha, "Macromolecular contrast agents for optical imaging of tumors: Comparison of indotricarbocyanine-labeled human serum albumin and transferring," *Photochem. Photobiol.,* vol. 72, pp. 234–241, Jun. 2000.

[39] V. Ntziachristos, A. G. Yodh, M. Schnall, B. Chance, "Concurrent MRI and diffuse optical tomography of breast after indocyanine green enhancement," *Proc. Natl. Acad. Sci. U.S.A.,* vol. 97, pp. 2767–2772, Mar. 2000.

[40] J. Yguerabide, E. E. Yguerabide, "Light-scattering submicroscopic particles as highly fluorescent analogs and their use as tracer labels in clinical and biological applications, I. Theory," *Anal. Biochem.,* vol. 262, pp. 137–156, Sep. 1998.

[41] J. Yguerabide, E. E. Yguerabide, "Light-scattering submicroscopic particles as highly fluorescent analogs and their use as tracer labels in clinical and biological applications, II. Experimental characterization," *Anal. Biochem.,* vol. 262, pp. 157–176, Sep. 1998.

[42] P. N. Prasad, in *Nanophotonics*, John Wiley & Sons, Eds., Hoboken, New Jersey, 2004, (a) p. 30; (b) p. 138; (c) 130; (d) p. 142; (e) p. 143; (f) pp.143 – 144; (g) p. 133.

[43] S. Link, Z. L. Wang, M. A. El-Sayed, "Alloy Formation of Gold-Silver Nanoparticles and the Dependence of the Plasmon Absorption on Their Composition," *J. Phys. Chem. B*, vol. 103, pp. 3529-3533, Mar. 1999.

[44] Y. Xu, G. Lei, A. C. Booker, K. A. Linares, D. Fleming, K. Meehan, G. Q. Lu, N. G. Love, B. J. Love, "Maximizing dye fluorescence via incorporation of metallic nanoparticles in solution," in *Lab-on-a-Chip: Platforms, Devices, and Applications, Proceedings of SPIE*, vol. 5591, L. A. Smith, D. Sobek, Eds. Bellingham, WA, 2004, pp. 174–184.

[45] J. Gersten, A. Nitzan, "Spectroscopic properties of molecules interacting with small dielectric particles*," J. Chem. Phys*., vol. 75, pp. 1139-1152, Aug. 1981.

[46] A. Campion, A. R. Gallo, C. B. Harris, H. J. Robota, P. M. Whitmore, "Electronic energy transfer to metal surfaces: A test of classical image dipole theory at short distances," *Chem. Phys. Lett.*, vol. 73, pp. 447-450, Aug. 1980.

[47] S. Link, M. A. El Sayed, "Spectral properties and relaxation dynamics of surface plasmon electronic oscillations in gold and silver nanodots and nanorods," *J. Phys. Chem. B,* vol. 103, pp. 8410-8426, Aug. 1999.

[48] P. Mulvaney, "Surface plasmon spectroscopy of nanosized metal particles," *Langmuir*, vol. 12, pp. 788-800, Feb. 1996.

[49] K. Torigoe, Y. Nakajima, K. Esumi, "Preparation and characterization of colloidal silver-platinum alloys," *J. Phys. Chem*., vol. 97, pp. 8304-8309, Apr. 1993.

[50] J. R. Lakowicz, Y. Shen, S. D'Auria, J. Malicka, J. Fang, Z. Gryczynski, I. Gryczynski, "Radiative decay engineering. 2. Effects of silver island films on fluorescence intensity, lifetimes, and resonance energy transfer," *Anal. Biochem.*, vol. 301, pp. 261-277, Jan. 2002.

[51] Fluorescence quantum yield standards. [Online]. Available : http://www.iss.com/Resources/yield.html.

[52] C. Vauthier, C. Schmidt, P. Couvreur, "Measurement of the density of polymeric nanoparticulate drug carriers by isopycnic centrifugation," *J. Nanoparticle Res*., vol. 1, pp. 411-418, Apr. 1999.